Journal of Science and Technology in Civil Engineering NUCE 2019. 13 (1): 21–32

EVALUATION OF ULTIMATE BENDING MOMENT OF CIRCULAR CONCRETE–FILLED DOUBLE SKIN STEEL TUBES USING FINITE ELEMENT ANALYSIS

Vu Quang Viet[a], Hoang Ha[b], Pham Thai Hoan[c,*]

[a]*Faculty of Civil Engineering, Vietnam Maritime University, 484 Lach Tray road, Le Chan district, Hanoi, Vietnam*
[b]*Vietnam Acapel Architects Ltd. Company, Nguyen Huy Tuong street, Thanh Xuan district, Hanoi, Vietnam*
[c]*Faculty of Building and Industrial Construction, National University of Civil Engineering, 55 Giai Phong road, Hai Ba Trung district, Hanoi, Vietnam*

Article history:
Received 19 November 2018, Revised 04 January 2019, Accepted 04 January 2019

Abstract

In this study, the ultimate bending moment of circular concrete-filled double skin steel tubes (CFDSTs) was investigated. A CFDSTs made of two concentric circular steel tubes with concrete infill and M16 shear connector system was fabricated. The four-point bending test of the 10 m long CFDST consisting of outer and inner steel tubes with 914.4 mm and 514.4 mm in diameter, respectively, was carried out and the ultimate bending moment of the CFDST was investigated. A finite element (FE) simulation of the CFDSTs subjected to bending was developed using the commercial software ABAQUS and the accuracy of the developed FE model was verified by comparing to the experimental result. The ultimate bending moment of CFDSTs was then evaluated with respect to different concrete infill compressive strengths and yield strengths of the steel tubes. The corresponding design ultimate bending moments of the CFDST with regard to the design codes AISC and EC4 were also computed. The results revealed that EC4 and AISC can accurately predict the ultimate moment capacities of the CFDST with shear connector.

Keywords: ultimate bending moment; concrete-filled double skin tube; shear connector system; finite element analysis.

https://doi.org/10.31814/stce.nuce2019-13(1)-03

1. Introduction

Fully concrete-filled steel tubes (CFST) have been widely used in the past few decades due to their better structural performance than that of pure steel or pure reinforced concrete. While the hollow steel tube acts as formwork as well as reinforcement for the concrete, the concrete infill eliminates or delays the local buckling of steel hollow tube, and increases significantly the ductility of the section. The use of CFST in construction has proven to be economic in material as well as leading to rapid construction process and thus additional cost savings [1].

Recently, concrete-filled double skin steel tubes (CFDST), which not only provide the advantages of concrete-filled steel tubes (CFST) but also supplement the weaknesses of CFST, have been extensively developed. CFDST sections consist of two steel tubes, an outer and an inner tube, with concrete

*Corresponding author. *E-mail address:* hoanpt@nuce.edu.vn (Hoan, P. T.)

sandwiched between the tubes. Advantages of CFDST tubes are over CFST include: increase in section modulus; enhancement in stability; lighter weight; good damping characteristics and better cyclic performance. It is expected that the CFDST columns can obtain a higher fire resistance period than the CFST columns, due to the inner tubes of the composite columns being protected by the sandwiched concrete during the fire. It is thus expected that CFDST has a potential of being used in building structures. Furthermore, the space in the inner tube can be utilized for other purposes such as for electrical cables. Thus, researches related to CFDSTs have been widely implemented. For instance, experimental researches on beams, columns, and beams-columns made of CFDSTs with various cross-sections were conducted by Tao and Han [2]. Eom et al. [3] performed an experimental investigation on CFDSTs with and without a joint subjected to bending. Experiment and analysis studies on CFDSTs under cyclic and long-term sustained loadings were implemented by Han [4, 5]. By performing experimental researches, Wang [6] and Huang [7] investigated the behavior of CFDSTs under collision and torsion loads, respectively. Regarding analytical studies, Pagoulatou [8] examined the behavior of CFDST stub columns under concentric axial compression loads, and then he suggested a new expression for evaluation of the strength of CFDSTs corresponding to EC4 [9]. By using finite element analysis (FEA), Huang [10] investigated the effects of important parameters which are used to determine sectional capacities of CFDST stub columns. In the other hand, many researchers have investigated the CFDST subjected to only pure bending [11–15], however, comprehensive studies in ultimate bending moment of CFDST, especially with a full scale CFDST, have not been reported so far.

This study aims to investigate the behavior of a full scale CFDST by conducting a four-point bending test. The developed FE model is used to evaluate the ultimate bending moment capacity of this CFDST with respect to different concrete infill compressive strengths and yield strengths of the steel tubes. The corresponding design ultimate bending moments according to AISC and EC4 are also computed for the purpose of comparison.

2. Experimental program

2.1. Design of CFDST

Fig. 1 illustrates the design of CFDST used in this study. The CFDST with the length of 10 m consists of outer and inner steel tubes with the diameter of 914.4 mm and 514.4 mm, respectively. The designed thicknesses of the outer and inner steel tubes were 8 mm and 6 mm, respectively. A

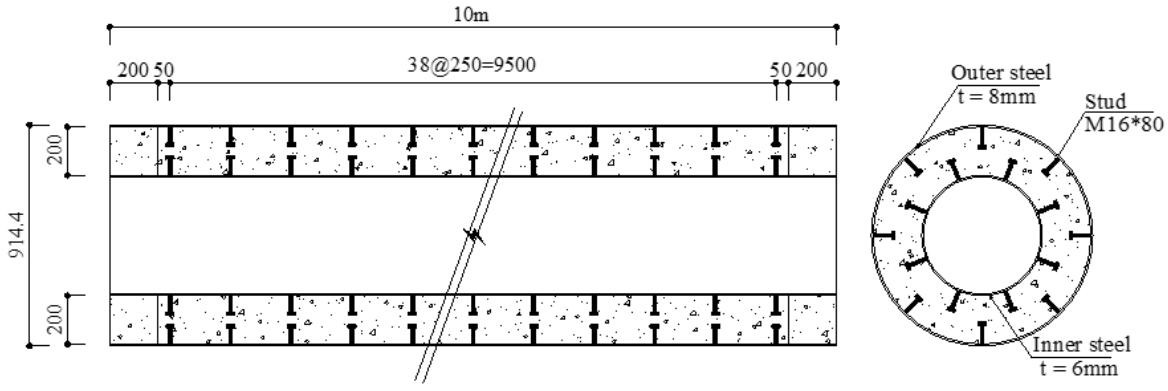

Figure 1. Geometry description of CFDST

layer of 200-mm-thick concrete was filled into the space between the outer and inner steel tubes. A shear connector system of M16 studs was designed and used in order to cause the composite action between the concrete and steel tubes. On the cross-section of the tubes, sixteen studs were welded between the inner and outer steel tubes, while along the longitudinal section of the tubes, studs were placed at 250 mm spacing as shown in Fig. 2. The design of CFDST including the shear connector system conforms to the requirement of the steel structure design standards [9, 16].

Figure 2. Detail of the steel tubes and shear connector system

The material properties of the concrete and the steel tubes are shown in Table 1. Tensile coupon tests were employed to obtain the steel material properties, whilst concrete cylinder tests were used to obtain the concrete material properties of the CFDST. The concrete specimens were tested at 28 days after casting.

Table 1. Material properties of steel tubes and concrete

Item	Yield strength F_y (MPa)	Ultimate strength F_u (MPa)	Compressive strength f_c' (MPa)	Young modulus E (MPa)
Outer steel tube (8 mm)	486.5	533.9	-	205000
Inner steel tube (6 mm)	467.6	517.8	-	205000
Concrete	-	-	48.9	-

2.2. Experimental setup and result

Four-point bending test was carried out to evaluate the ultimate bending moment of the designed CFDST. The specimen was tested by hydraulic jacks with a loading capacity of 5000 kN. The loads were applied on the specimen at two positions of 750 mm away from the center of the CFDST on both sides. Loading and boundary pads with the same 25 mm of thickness were placed to prevent stress concentration at the loading positions and the supporting ends. Three Linear Variable Displacement Transducers (LVDT) were placed along the bottom of the specimens in a pure bending segment to measure the mid-span vertical displacement of the tube. Hinge and roller conditions were applied to the bottom of the boundary pads. The configuration and arrangement of the experimental setup are illustrated in Fig. 3.

The bending experiment was undertaken with displacement control at the velocity of 2 mm/min in the elastic region and 4 mm/min in the plastic region until the specimen collapsed. The applied

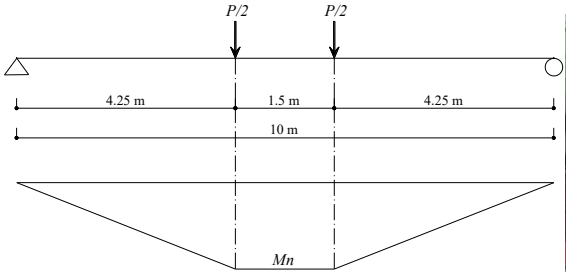

(a) Loading diagram

(b) Experimental arrangement

(c) Roller support end

(d) Hinge support end

Figure 3. Experimental setup on CFDST

load P and vertical displacement at the mid-span of CFDST were measured during the test and the corresponding bending moment M at the mid-span section was also computed based on the loading diagram in Fig. 3(a), as follows:

$$M = \frac{P}{2} l_1 + \frac{sw}{8} l_2^2 \tag{1}$$

where $l_1 = 4.25$ m, $l_2 = 10$ m, and sw is the self-weight of the CFDST ($sw = 13.5$ kN/m).

Fig. 4 shows the failure mode and Fig. 5 presents the bending moment-vertical displacement curve at the mid-span of the specimen. It can be seen from these figures that the CFDST specimen

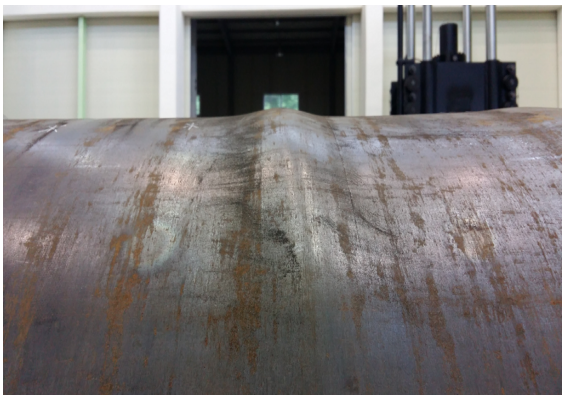

Figure 4. Failure mode of CFDST

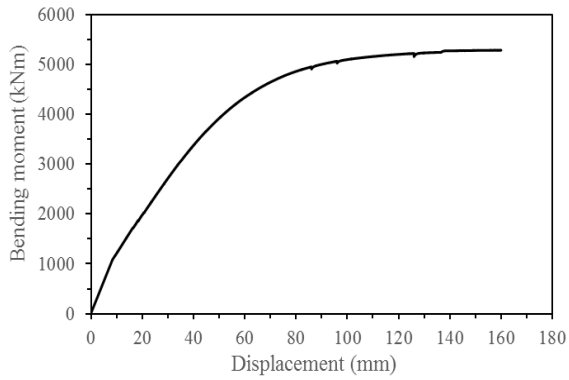

Figure 5. Moment-displacement behavior

collapsed due to the local buckling of the outer steel tube and the corresponding failure load is 2486 kN. The applied load at the failure is considered ultimate bending load of the CFDST obtained from the experiment in this study, leading to the ultimate bending moment of 5299 kNm.

3. Finite element simulation

3.1. Finite element modeling

In order to investigate and evaluate the ultimate bending moment of CFDSTs with respect to different concrete infill compressive strength and steel tubes yield strength regardless to conducting such uneconomic experiments, the commercial software ABAQUS [17] was used to simulate the four-point bending test of CFDST, which was carried out in the present study. For finite element (FE) model, 8-node solid elements (C3D8R) were used for the steel tubes, steel pads, and concrete of CFDST, whereas truss elements (T3D2) were used to model the M16 shear connector system. The appropriate element mesh size of 50 mm was chosen for the FE model by performing the sensitivity analysis. The interaction between concrete and steel tubes was modeled using the *CONTACT PAIR option, which is a surface-to-surface contact type available in ABAQUS [12]. Two types of surfaces including slave and master surfaces were required to define this contact option. It was suggested that the slave surface should be assigned to a softer material in order to limit the numerical errors, thus the steel tubes were assigned as master surfaces while the concrete was set as slave surfaces. The normal and tangent behavior between the slave and master surfaces were modeled by adopting the hard contact and the Coulomb friction model with a friction coefficient of 0.1, respectively. For the contact between the shear connectors and the concrete, the M16 studs were assumed to be completely bonded to the concrete and were simulated using the EMBEDDED option. In addition, the contact between the pads and outer steel tubes was modeled by using the TIE option. The loads were applied in one row at the top middle of the loading pads, which were installed at 750 mm away from the center of the CFDST on both sides. The hinge and roller conditions were applied to the middle points (reference points) of the boundary pads. Fig. 6 shows the detail modeling of the components and the FE model.

Concerning the material models, the plasticity model was used for steel tubes and the concrete damaged plasticity model was utilized for concrete infill. Noted that the concrete damaged plasticity model proposed by Lubiner et al. [18] and by Lee and Fenves [19], which can model the inelastic response of concrete, is available in ABAQUS. Fig. 7 shows the stress-strain curves of materials used in this study, where the material parameters obtained from the coupon tests in Table 1 were adopted. The stress-strain curve of concrete was constructed by using T'sai concrete model [20]. It is worth noting that the missing parameters of concrete material from the coupon test, such as strain values at compressive strength (ε_c) and at failure (ε_{c_1}) and Young modulus (E), were taken based on the concrete compressive strength according to EC2 [9] as 0.002, 0.003, and 37 GPa, respectively. The Poisson's ratio was taken to be 0.2 for concrete and 0.3 for steel.

3.2. Finite element analysis result

During the FE analysis, the stress distributions on the whole CFDST can be captured and the relationship between the bending moment and displacement at the mid-span of the CFDST can be obtained. Fig. 8 shows the stress contour of the whole CFDST at the failure, while Fig. 9 presents the comparison of the bending moment-displacement at mid-span behavior obtained from FE analysis and experiment. As can be seen from Fig. 9 that the bending moment-displacement curve from FE

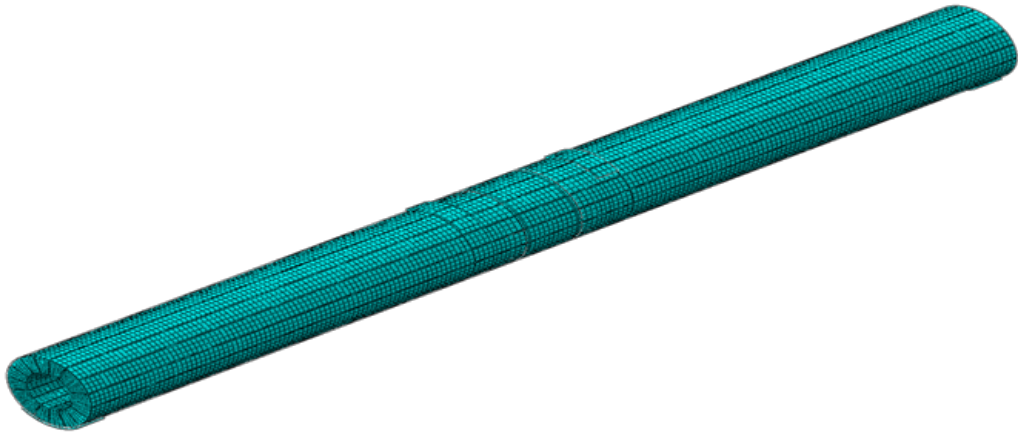

(a) Finite element model

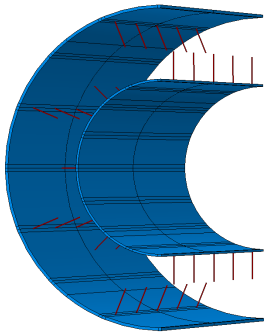

(b) Shear connector

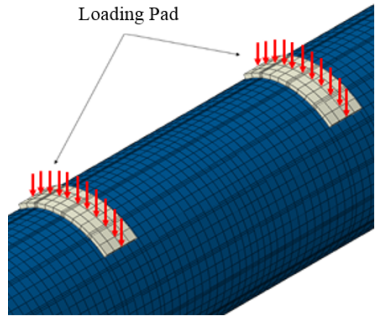

(c) Loading pads

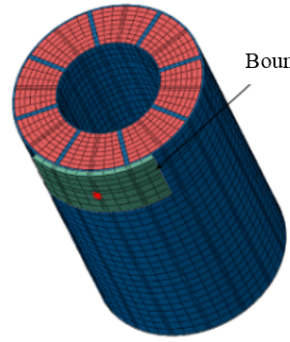

(d) Boundary pad

Figure 6. Details of components and FE model

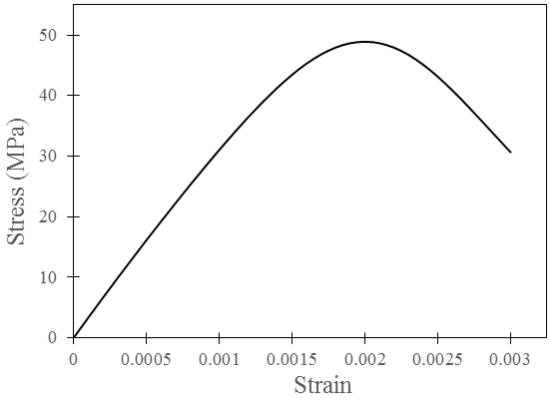

(a) Stress-strain curve of concrete

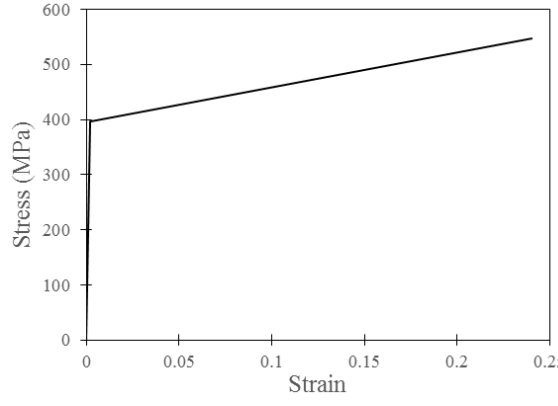

(b) Stress-strain curve of steel

Figure 7. Material models

analysis is in good agreement with that obtained from the experiment of CFDST. Not only the shape of the curve but also the ultimate moment $M_{u.ana}$ = 5461 kNm obtained from FE analysis agrees

well with that of the experiment with a relative error of 3.1%. The observed result indicates that the developed FE model can be used to accurately simulate the four-point bending test of CFDST.

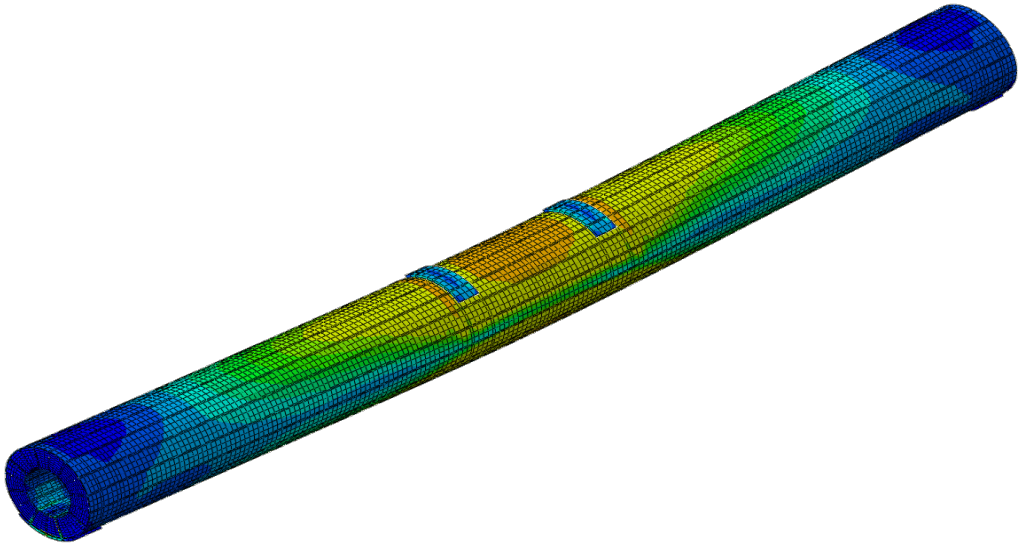

Figure 8. Stress distributions of the CFDST

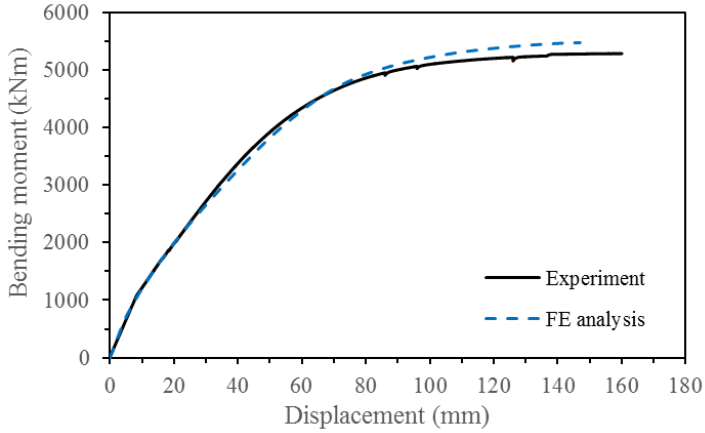

Figure 9. Comparison between FE analysis and experiment result

4. Ultimate bending moment of CFDST

In order to evaluate the ultimate bending moment of CFDST with respect to different concrete compressive strengths and steel yield strengths, FE simulations of four-point bending test of CFDST with various values of concrete and steel yield strengths were conducted. To examine the effect of concrete compressive strength on the ultimate bending moment of CFDST, four different values of 40 MPa, 60 MPa, 80 MPa, and 100 MPa were utilized, while the yield strengths of steel tubes were kept unchanged as the value obtained from the steel coupon tests. In contrast, the effect of the yield strength of steel tubes was considered by varying these strength values while keeping the concrete

material parameters unchanged. Since the higher yield strength of steel when compared to the used steel materials in the test may lead to the high strength steel type, which shows different stress-strain behavior, only lower yield strength values were used in parametric study. Due to the fact that the values of yield strength of outer and inner steel tubes used in the test were different, the reduced ratios of 1.2, 1.4, and 1.6 for both steel yield strengths of outer and inner tubes were used in order to obtain a meaningful comparison. Noted that the chosen concrete compressive strength and reduced ratios of steel yield strength represent to the properties of commonly used concrete and steel materials in real structures.

4.1. Effect of concrete compressive strength

Fig. 10 presents the bending moment-displacement curves of CFDST with different concrete compressive strengths obtained from the FE analyses. Table 2 lists the material properties used in FE analyses and the corresponding ultimate bending moments of CFDST.

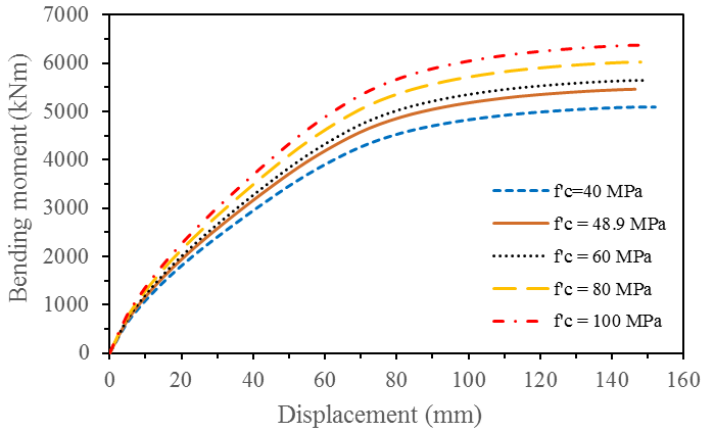

Figure 10. Effect of concrete compressive strength on moment-displacement curve

Table 2. Ultimate bending moments with respect to different concrete strengths

F_y/F_u of outer steel tube (MPa)	F_y/F_u of inner steel tube (MPa)	f'_c (MPa)	M_u (kNm)
486.5/ 533.9	467.6/ 517.8	40	5092
		48.9	5461
		60	5644
		80	6024
		100	6372

As can be seen in Fig. 10 and Table 2 that while the shapes of moment-displacement curve at mid-span of CFDST are almost similar, the ultimate bending moment of CFDST increases with the increment of concrete compressive strength. The similar shapes of moment-displacement curve at mid-span of CFDST indicate that the concrete infill has strong influence on the bending behavior of CFDST in both elastic and plastic regions. It is also interesting to observe that the increase of ultimate bending moment of CFDST with respect to the increasing concrete compressive strength is almost linear, as shown in Fig. 11.

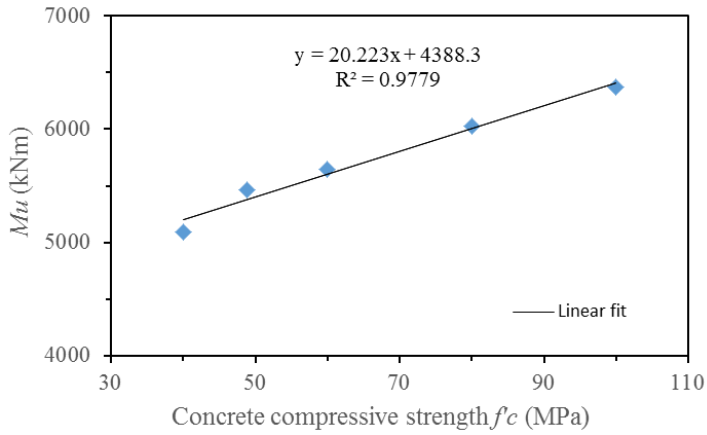

Figure 11. Effect of concrete compressive strength on ultimate bending moment

4.2. Effect of yield strength of steel tubes

Fig. 12 shows the moment-displacement curves of CFDST with different yield strength values of outer and inner steel tubes obtained from the FE analyses. Table 3 presents the material properties used in FE analyses and the corresponding ultimate bending moments of CFDST.

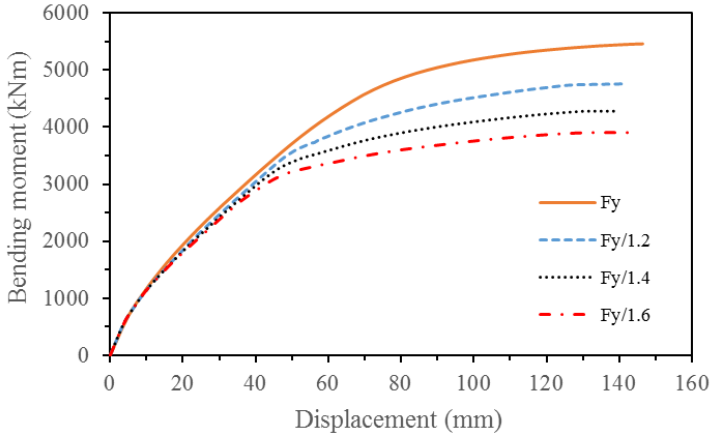

Figure 12. Effect of yield strength of steel tubes on moment-displacement curve

Table 3. Ultimate bending moments with respect to different strengths of steel tubes

f_c' (MPa)	Reduced ratio of Fy	F_y/F_u of outer steel tube (MPa)	F_y/F_u of inner steel tube (MPa)	M_u (kNm)
48.9	1	486.5/ 533.9	467.6/ 517.8	5461
	1.2	405.4/ 444.9	389.7/ 431.5	4764
	1.4	347.5/ 381.4	334.0/ 369.9	4281
	1.6	304.1/ 333.7	292.3/ 323.6	3905

It is seen from Table 3 and Fig. 12 that the ultimate bending moment of CFDST decreases as the yield strength of steel tubes decreases, whereas the load-displacement curves at mid-span of CFDST

in the elastic region are almost identical. This observed result reveals that the yield strength of outer and inner steel tubes has strong influence on the ultimate bending moment of CFDST but the influence just appears in the plastic region, while in the elastic region the yield strength of steel tubes shows trivial effect on the bending behavior of CFDST. It is also worth to mention that the reduced ratio of ultimate bending moment, which represents the decreasing ratio of ultimate bending moments of CFDST when the yield strength of steel tubes decreases, exhibits an exactly linear decrease with respect to the decreasing yield strength of steel tubes, as illustrated in Fig. 13.

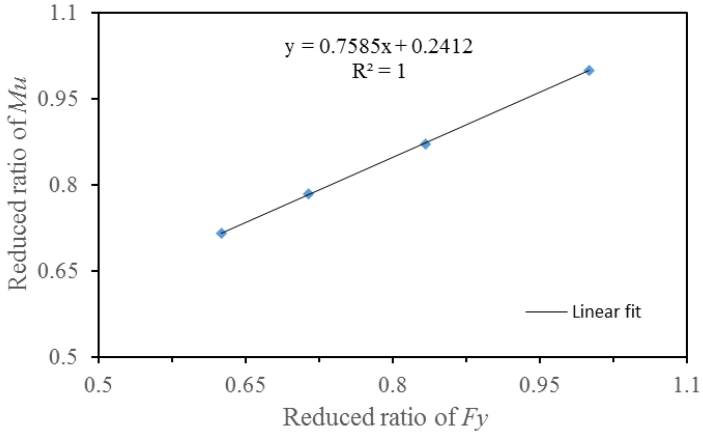

Figure 13. Effect of yield strength of steel tubes on reduced ultimate bending moment

4.3. Recommendation on the design bending moment capacity of CFDST

Both popular design codes Eurocode 4 (EC4) [9] and AISC [16] provide parallel two methods for the evaluation of the nominal moment capacity of fully concrete filled steel tube (CFST), which are the strain compatibility method (SCM) and the plastic stress distribution method (PSDM). Using the same principle of the codes for CFST, the PSDMs in both aforementioned codes were utilized to predict the nominal moment capacity of CFDST in this study. Noted that the nominal moment capacity of a cross-section corresponds to the bending ultimate moment of the tube (M_u) in this study. Fig. 14 illustrates the calculation principle of nominal moment capacity based on the plastic stress distribution method provided in EC4. The plastic neutral axis (PNA) of the cross-section of the tube

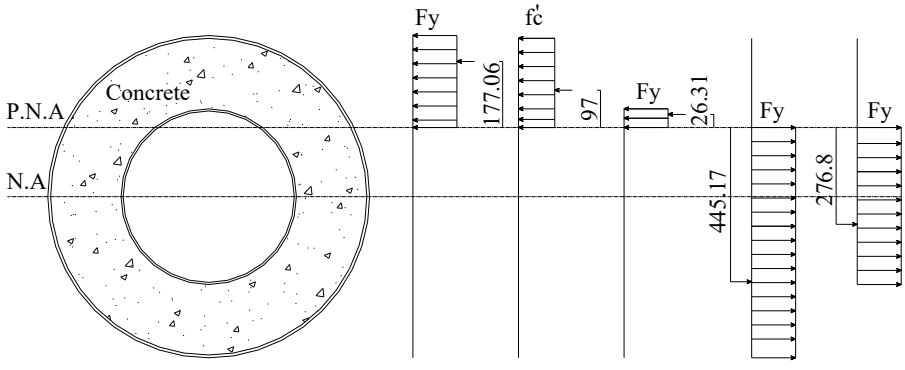

Figure 14. Plastic stress distribution of CFDST (EC4)

divides the section into two parts, where the total of compressive stresses of steel and concrete in compression zone (upper part) equals to the total of tensile stresses of steel in tension zone (lower part). The nominal moment capacity M_u of the cross-section is determined based on the total moment caused by these stresses in both upper and lower parts with respect to plastic neutral axis (so called M_p) by multiplying by a load and resistance factor for bending ϕ_b. According to EC4, the compressive stress of concrete in compression zone is taken as compressive strength of concrete, both compressive and tensile stresses of steel are taken as yield strength of steel, while the load and resistance factor for bending is 0.9. The PSDM in AISC is same with that in EC4 except the compressive stress of concrete is taken as 0.95 compressive strength ($0.95f_c'$).

In present study, the nominal moment capacity of the designed CFDST was predicted using the aforementioned method according to both EC4 and AISC codes. The geometric parameters of the CFDST and the properties of materials used in the test were utilized in the calculation. The computed nominal moment capacity (so called ultimate bending moment) of the CFDST according to both codes are listed in Table 4, together with those obtained from the test and FE analysis result. It is seen from this table that the ultimate bending moments calculated using both codes EC4 and AISC are in good agreement with that obtained from the experiment. The prediction recommended by EC4 method is slightly closer to the test result than that recommended by AISC method since EC4 method presumes that the concrete stress is f_c' instead $0.95f_c'$ used in the AISC method.

Table 4. Ultimate bending moment of CFDST

Method	M_u (kNm)	$M_u/M_{u.exp}$
Experiment	5299*	1.00
FE analysis	5461	1.03
AISC	4947	0.93
EC4	4973	0.94

*$M_{u.exp}$: the ultimate bending moment obtained from experiment.

5. Conclusions

In this study, a concrete-filled double circular skin steel tubes was designed. The flexural behavior and bending ultimate moment of the CFDST were investigated through the experiment and FE analysis. The following conclusions can be withdrawn:

- The developed FE model can be used to accurately simulate the four-point bending test of CFDST.

- The infilled concrete strength has strong influence on the bending behavior of CFDST in both elastic and plastic regions. The increase of bending ultimate moment of CFDST with respect to the increasing concrete compressive strength is almost linear.

- The yield strength of outer and inner steel tubes has strong influence on the bending ultimate moment of CFDST but the influence just appears in the plastic region, while in the elastic region the yield strength of steel tubes shows trivial effect on the bending behavior of CFDST. The reduced ratio of bending ultimate moment exhibits an exactly linear decrease with respect to the decreasing yield strength of steel tubes.

- The nominal moment capacity of the CFDST predicted by EC4 method is slightly closer to the test result than that predicted by AISC method.

Acknowledgement

The study presented in this paper was financially supported by National University of Civil Engineering through Grant 75-2019/KHXD and XD-2019-29. The financial support is greatly appreciated.

References

[1] Han, L.-H., Huang, H., Tao, Z., Zhao, X.-L. (2006). Concrete-filled double skin steel tubular (CFDST) beam–columns subjected to cyclic bending. *Engineering Structures*, 28(12):1698–1714.

[2] Tao, Z., Han, L.-H. (2006). Behaviour of concrete-filled double skin rectangular steel tubular beam–columns. *Journal of Constructional Steel Research*, 62(7):631–646.

[3] Eom, S.-S., Vu, Q.-V., Choi, J.-H., Park, H.-H., Kim, S.-E. (2019). Flexural behavior of concrete-filled double skin steel tubes with a joint. *Journal of Constructional Steel Research*, 155:260–272.

[4] Han, L.-H., Tao, Z., Liao, F.-Y., Xu, Y. (2010). Tests on cyclic performance of FRP–concrete–steel double-skin tubular columns. *Thin-Walled Structures*, 48(6):430–439.

[5] Han, L.-H., Li, Y.-J., Liao, F.-Y. (2011). Concrete-filled double skin steel tubular (CFDST) columns subjected to long-term sustained loading. *Thin-Walled Structures*, 49(12):1534–1543.

[6] Wang, R., Han, L.-H., Tao, Z. (2015). Behavior of FRP-concrete-steel double skin tubular members under lateral impact: Experimental study. *Thin-Walled Structures*, 95:363–373.

[7] Huang, H., Han, L. H., Zhao, X. L. (2013). Investigation on concrete filled double skin steel tubes (CFDSTs) under pure torsion. *Journal of Constructional Steel Research*, 90:221–234.

[8] Pagoulatou, M., Sheehan, T., Dai, X. H., Lam, D. (2014). Finite element analysis on the capacity of circular concrete-filled double-skin steel tubular (CFDST) stub columns. *Engineering Structures*, 72: 102–112.

[9] Eurocode 4 (2004). *Design of composite steel and concrete structures. Part 1-1: General rules and rules for buildings*. EN 1994-1-1, European Committee for Standardization.

[10] Huang, H., Han, L.-H., Tao, Z., Zhao, X.-L. (2010). Analytical behaviour of concrete-filled double skin steel tubular (CFDST) stub columns. *Journal of Constructional Steel Research*, 66(4):542–555.

[11] Chen, J., Wang, J., Xie, F., Jin, W.-l. (2016). Behavior of thin-walled dodecagonal section double skin concrete-filled steel tubes under bending. *Thin-Walled Structures*, 98:293–300.

[12] Uenaka, K., Kitoh, H., Sonoda, K. (2008). Concrete filled double skin tubular members subjected to bending. *Steel and Composite Structures*, 8(4):297–312.

[13] Shimizu, M., Tatsumi, F., Ishikawa, T., Hattori, A., Kawano, H. (2013). Experimental study on ultimate strength of concrete filled double tubular steel with shear connector. *International Journal of Steel Structures*, 13(1):49–54.

[14] Zhao, J. L., Teng, J. G., Yu, T., Li, L. J. (2016). Behavior of Large-Scale Hybrid FRP–Concrete–Steel Double-Skin Tubular Beams with Shear Connectors. *Journal of Composites for Construction*, 20(5): 04016015.

[15] Wang, F., Young, B., Gardner, L. (2017). Tests on concrete-filled double skin tubular beams with circular stainless steel outer tubes. *Eurosteel 2&3: 1996-2005*, 1(2-3):1996–2005.

[16] ANSI/AISC 360-10 (2010). *Specification for structural steel buildings*. American Institute of Steel Construction.

[17] ABAQUS (2014). *Analysis user's manual version 6.14*. Dassault Systems.

[18] Lubliner, J., Oliver, J., Oller, S., Onate, E. (1989). A plastic-damage model for concrete. *International Journal of Solids and Structures*, 25(3):299–326.

[19] Lee, J., Fenves, G. L. (1998). Plastic-damage model for cyclic loading of concrete structures. *Journal of Engineering Mechanics*, 124(8):892–900.

[20] Tsai, W. T. (1988). Uniaxial compressional stress-strain relation of concrete. *Journal of Structural Engineering*, 114(9):2133–2136.